# NiO growth on Ag(001): A layer-by-layer vibrational study

K. L. Kostov,[1,2] F. O. Schumann,[1] S. Polzin,[1] D. Sander,[3] and W. Widdra[1,3]
[1]*Institute of Physics, Martin-Luther-Universität Halle-Wittenberg, 06120 Halle, Germany*
[2]*Institute of General and Inorganic Chemistry, Bulgarian Academy of Sciences, 1113 Sofia, Bulgaria*
[3]*Max Planck Institute for Microstructure Physics, 06120 Halle, Germany*
(Received 18 March 2016; revised manuscript received 20 June 2016; published 26 August 2016)

The vibrational properties of NiO(001) films on Ag(001) with thicknesses up to 50 monolayers (ML) are characterized with high-resolution electron energy loss spectroscopy (HREELS). For NiO growth at 300 K, four different coverage regions are distinguished by HREELS. The film-thickness-dependent Fuchs-Kliewer (FK) phonon frequency shifts and intensity changes are identified from the NiO monolayer to bulklike thick films. Characteristic changes of the vibrational properties are analyzed to resolve restructuring processes during annealing and thermal decomposition of NiO films. A quantitative comparison of the experimental data, including a line shape analysis, with the calculated loss function based on dielectric theory reveals an excellent agreement between the bulk and the NiO(001) thin film phonon properties for film thicknesses above 15 ML. In contrast, a strong FK phonon softening is observed for thin films below 5 ML that cannot be explained by dielectric theory nor phonon standing waves. This softening is attributed to the presence of surface stress, which results from the −2% lattice mismatch between NiO and Ag.

DOI: 10.1103/PhysRevB.94.075438

## I. INTRODUCTION

The interplay between lattice mismatch and surface stress, on the one hand, and surface lattice dynamics and surface electronic properties, on the other hand, is crucial for many thin and heterostructure systems. In particular, the relation between film strain, stress, and phonon softening or phonon hardening in thin films is prerequisite for the deeper understanding of interfacial properties of oxide surfaces with prominent examples in oxide and multiferroic heterostructures. The understanding of this interplay has also far-reaching implications for the widespread application of oxide interfaces and might lead to a controlled material engineering in spin-dependent transport and two-dimensional electron systems [1–3]. However, the understanding of lattice dynamics in oxides near interfaces is still in its infancy. Experimental studies that address the interrelation between thin film strain, static thin film stress, and resulting lattice dynamics are still very scarce. This lack of experimental data originates from the difficulty to address surface stress and lattice dynamics with the required accuracy under *in situ* growth conditions. For oxide thin films, the first layer-dependent surface stress data have been published for NiO(001), $BaTiO_3$(001), and $SrTiO_3$(001) thin films just recently [4,5]. In the present paper, we will address the thickness-dependent lattice dynamics of ultrathin NiO films with varying strain and compare it to surface stress data. By this approach, we identify surface stress as a possible reason for the intriguing softening of phonons in the ultrathin film limit.

In detail, we report a comprehensive layer-dependent lattice dynamics study for NiO(001) on Ag(001) from NiO monolayer structures to NiO(001) films of 50 monolayers (ML), defined as multiples of a single layer of approximately coplanar $Ni^{2+}$ and $O^{2-}$ ions, with an average NiO interlayer spacing of 2.04 Å [4]) thickness. A comprehensive characterization of the lattice dynamics within the strained oxide thin film is achieved, also by discussing earlier studies on the surface phonon dispersion of thick (25 ML) and ultrathin (4 ML) NiO(001) films [6,7]. In the present paper, NiO films on Ag(001) are studied in a wide range of thicknesses between 0 and 50 ML using high-resolution electron energy loss spectroscopy (HREELS). The HREELS data are discussed quantitatively with respect to phonon frequencies, lifetime broadening, and intensities within the classical dielectric theory in combination with a standing wave approach for the suppressed phonon propagation along the film normal. A result of our paper is that we find characteristic phonon shifts for each layer together with a monotonically increase of the oscillator strength with film thickness. This allows identifying restructuring processes during annealing and thermal decomposition of NiO films from the corresponding characteristic changes of the vibrational spectra, which is not accessible by other methods.

The small lattice mismatch of only ∼−2% between NiO and Ag allows to grow well ordered and smooth NiO(001) films on an Ag(001) surface by evaporation of Ni in an oxygen atmosphere [8,9]. At 300 K, NiO grows in a layer-by-layer mode for coverages beyond a NiO bilayer. The first monolayer forms an interface phase, which is characterized by an uniaxially distorted hexagonal precursor [10–13]. Above 0.8 ML, (1 × 1)-NiO(001) two monolayer high islands start to nucleate, as observed by scanning tunneling microscopy (STM) [13,14], which cover the Ag(001) substrate completely at 2 ML. The interlayer distances of NiO films between 2 and 5 ML are close to that of bulk NiO (2.09 Å), whereas the in-plane parameters are matching the Ag(001) substrate. The latter arises from the pseudomorphic NiO growth on Ag(001) in this thin film limit [15,16]. In the thickness range between 5 and approximately 15 ML, the NiO films start to relax structurally. This can be ascribed to the reduction of film stress, which leads to the formation of a mosaic structure [15]. A quantitative determination of the growth-induced surface stress by the crystal bending technique revealed a positive (tensile) surface stress change for the initial NiO/Ag(001) interface formation and a strong negative (compressive) stress change up to 5 ML, which is due to lattice misfit [4]. Above

 

5 ML, the stress curve levels off, indicating the beginning of the structural (mosaic) relaxation processes [4,15].

## II. EXPERIMENTAL

The measurements have been performed in a multichamber ultrahigh vacuum (UHV) system with a base vacuum of $10^{-9}$ Pa. The Ag(001) sample preparation has been carried out by standard procedures, which include repeated cycles of $Ar^+$ sputtering (3 $\mu$A at 1 keV ion energy) and subsequent annealing at 700 K, as controlled by low-energy electron diffraction (LEED).

The HREEL spectrometer (Delta 05, Specs GmbH, Berlin, Germany) is located in a separate chamber. The electron scattering plane is adjusted to be parallel to the [110] direction, where the appropriate azimuthal orientation of the sample is controlled by LEED. The scattering geometry is characterized by an incidence angle of 60° with respect to the surface normal. All reported results are measured in the specular direction at a primary energy of 4 eV, if not stated otherwise. This setup results in an energy resolution of 1 meV ($\sim$8 cm$^{-1}$) at count rates up to $10^6$ s$^{-1}$ on well-ordered adsorbate layers [17–19]. In the present paper, the resolution is in the range of 1.5–2.5 meV (12–20 cm$^{-1}$), depending on the surface ordering. This resolution is similar to our recent paper on phonon dispersions of thick NiO layer on Ag(001) [6].

## III. RESULTS

### A. General aspects of NiO growth mechanism

The NiO layers with different thicknesses have been grown by reactive deposition of Ni onto atomically clean Ag(001) at 300 K in an oxygen atmosphere of 1–5 $\times$ $10^{-7}$ mbar. This ensures a complete oxidation of the nickel for Ni evaporation rates of 0.7 ML min$^{-1}$. The latter has been controlled by monitoring the (00) diffraction spot intensity of the Ag(001) surface during Ni evaporation using reflection medium-energy electron diffraction (RMEED) at a kinetic energy of 3 keV. A typical (00) intensity curve for NiO(001) growth at 300 K is shown in Fig. 1. The observed periodic oscillations indicate that the growth mechanism is layer by layer as the intensity maxima mark the completion of each subsequent monolayer (marked by vertical dashed lines). These oscillations allow for an exact thickness control of the thin films. No growth oscillations are visible up to 2 ML thickness. This is attributed to the complex and buckled surface morphology of the two-domain uniaxially compressed, quasihexagonal NiO monolayer with approximate (2 $\times$ $n$) periodicity. Furthermore, the formation of both NiO and Ag islands during the initial growth also leads to diffusive electron diffraction and an initial decrease of the (00) spot intensity in Fig. 1 [10,11,13].

Above a layer thickness of 1.5 ML, the (00) diffraction intensity starts to increase strongly. This and the decrease of the diffraction width [full width at half maximum (FWHM) in Fig. 1] is ascribed to the formation of well-ordered NiO(001)-(1 $\times$ 1) bilayer patches with an inhomogeneous lateral size distribution. as observed by STM [13]. At 2 ML NiO, the Ag(001) surface is fully covered [16], and the first intensity maximum is observed in Fig. 1, which coincides with a minimum spot width. Above 2 ML, periodic (00)

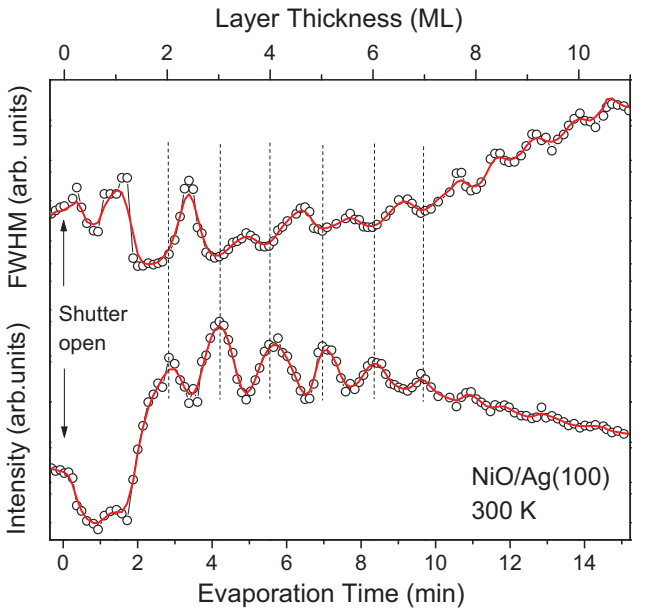


FIG. 1. NiO growth oscillations: (top) FWHM and (bottom) intensity of the (00) diffraction spot during Ni deposition in an $O_2$ atmosphere on Ag(001) at 300 K.

spot intensity oscillations are clearly observed with maxima at the completion of each monolayer (Fig. 1), as has been observed earlier [4]. This finding is in agreement with earlier conclusions that proposed the onset of a layer-by-layer NiO growth mechanism under these conditions [4,16,20]. At higher NiO thicknesses (>3 ML), the oscillation amplitude decreases continuously, although the oscillations are clearly visible until $\sim$10 ML (Fig. 1). The half width of the (00) spot also oscillates with increasing layer thickness, where minima are observed for each monolayer completion. However, the average FWHM increases with increasing the NiO thickness, which points to the accumulation of disorder with increasing thickness. Supporting arguments will be presented later in the context of the thermal stability of thick NiO films. There, annealing of the as-prepared NiO layers at higher temperatures leads to an increase of the electron reflectivity in HREELS, showing the improvement of the surface order.

The LEED patterns of the bare Ag(001) and NiO(001) films for six different thicknesses are shown in Fig. 2. From the clean Ag(001) substrate up to the growth of 5 ML NiO, a quadratic (1 $\times$ 1) pattern is preserved, as has been observed in previous studies [4,16]. This indicates pseudomorphic growth with a NiO lattice compression of 2%, maintaining the lattice parameter of Ag(001) [15,16]. The compressed NiO films begin to relax at about 5 ML, forming initially a mosaic structure with a characteristic LEED superstructure [Figs. 2(c)–2(e)]. A similar mosaic structure has been found for the growth of MgO on Ag(001) [21]. The results are in good agreement with the conclusion of Wollschläger *et al.* that the critical thickness of mosaic formation and, respectively, the onset of relaxation process is 5 ML of NiO film on Ag(001) [15]. The mosaic diffraction superstructure still exists up to 15 ML [Figs. 2(d) and 2(e)]. The detailed analysis of the superstructure indicates that the tilting angle of the mosaic

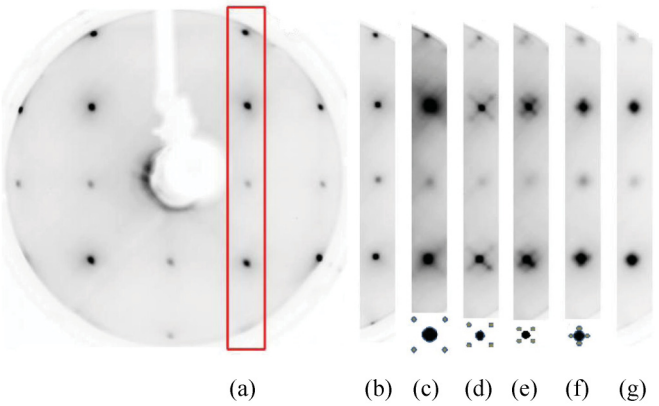


FIG. 2. The LEED patterns of clean Ag(100) surface (a) and after deposition of NiO(100) films of 2 ML (b), 5 ML (c), 10 ML (d), 15 ML (e), 20 ML (f), and 50 ML (g). The incident electron energy is 150 eV. For better visibility, the satellite structure around the principal spots is presented schematically below some of the patterns.

patches, with respect to the surface decreases [Figs. 2(c)–2(e)], as the satellite peaks move closer to the fundamental diffraction peaks [15]. This mosaic relaxation process of the NiO(001) film proceeds up to approximately 15–20 ML. Here, a new satellite superstructure is visible in LEED, which is 45° rotated, with respect to the mosaic superstructure, as can be identified in Figs. 2(f) and 2(g). These new diffraction features are attributed to a Moiré pattern [22] for two unrotated square lattices, with a 2% mismatch between Ag(001) and a relaxed NiO(001) thin film.

Figure 3 presents a series of HREEL spectra for NiO(001) thin films on Ag(001), with thicknesses between 1 and 50 ML. The most significant changes are visible for ultrathin NiO layers up to 2 ML. In this region, low-intensity vibrational features at about 125 and 300 $cm^{-1}$ are detected. These features are characteristic for the highly inhomogeneous morphology of the first oxide monolayer, as discussed above. The growing NiO bilayer islands dominate above 1.5 ML and are characterized by an intense peak at approximately 450 $cm^{-1}$. At film thicknesses above 2 ML, a two-peak phonon structure appears. The intensity and the frequency of the high-energy peak are changing with increasing NiO thickness (Fig. 3). The shape of the two-phonon peak structure converges with increasing film thickness to that of a NiO(001) single crystal [6]. Therefore, we attribute the low-intensity peak located at about 410–430 $cm^{-1}$ to the microscopic Wallis mode, representing a Ni-O vibration perpendicular to the surface [6,23], whereas the intense high-frequency peak is interpreted as macroscopic phonon polariton, known as Fuchs-Kliewer (FK) phonon [24,25]. For epitaxially fully compressed NiO films with a thickness of 2–5 ML, the FK phonon frequency changes significantly. However, a relative small frequency shift is detected in Fig. 3 for the coverage range above 5 ML, where, structurally, relaxation in the NiO films sets in. Note the reduced data acquisition time for films above 6 ML that resulted in a slightly reduced signal-to-noise ratio. Below, we discuss the vibrational NiO features within the different thickness regions in more detail.

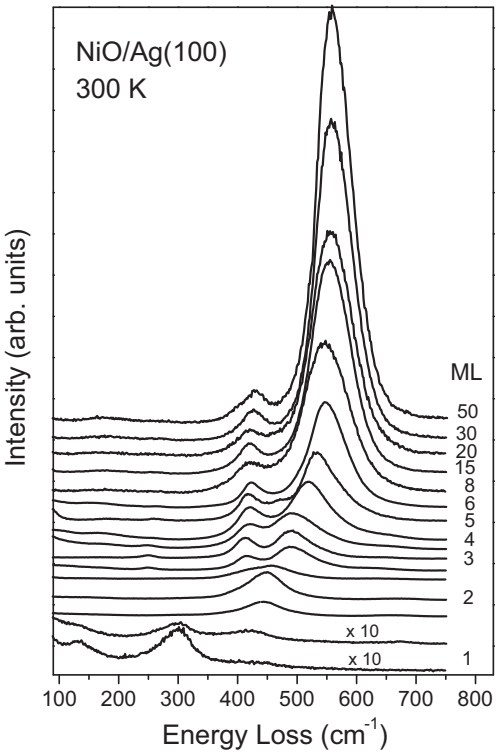


FIG. 3. The HREEL spectra of NiO on Ag(001) for NiO film thickness in the range of 1–50 ML. Primary energy 4 eV, $T = 300$ K.

### B. Interface formation: 0–2 ML NiO

For a NiO coverage of 0.3 ML, two intense loss peaks are present at 245 and 300 $cm^{-1}$ in the HREEL spectrum of Fig. 4(a). The dominant peak at 302 $cm^{-1}$ grows in intensity, with increasing coverage and characterizes the formation of the first NiO monolayer islands on Ag(001). The loss at 245 $cm^{-1}$ is tentatively assigned to adsorbed oxygen atoms in the vicinity of NiO monolayer islands (bound to island edges). This assignment is based on the relative high intensity at low NiO coverages and a decrease of intensity with completion of a full NiO monolayer. This assignment is further corroborated by the peak frequency, which is also in agreement with the O-Ag stretching vibration of adsorbed oxygen atoms on Ag(001) at 300 K [26]. The weak and broad features at about 500 and 600 $cm^{-1}$ exist only in the low submonolayer region. They are associated with a small concentration of defective Ni-oxide islands. These loss features disappear fully at higher NiO coverages (Fig. 4). The faint peak at ~150 $cm^{-1}$ is attributed to a characteristic peak of high phonon density for the bare Ag(001) regions [27].

The intensity of the loss peak at about 300 $cm^{-1}$ increases for higher NiO coverages of 0.8 and 1.0 ML [Figs. 4(b) and 4(c)]. In the same coverage range, an additional peak grows at about 125 $cm^{-1}$, which is observed only for the NiO monolayer. A low-intensity and broad loss at 430 $cm^{-1}$ already indicates the presence of some NiO bilayer islands [Figs. 4(b) and 4(c)]. This is in agreement with results of Caffio *et al.* showing that NiO bilayer islands start to nucleate at coverages of 0.7–0.8 ML [16]. As can be seen from Fig. 3, the vibrational spectra for 0.8 and 1.0 ML differ strongly from the energy-loss

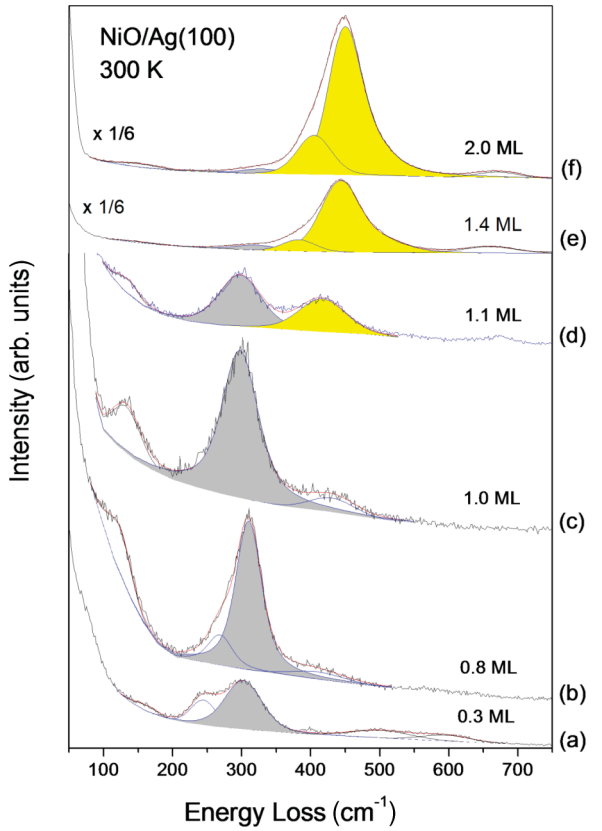


FIG. 4. Vibrational spectra of different NiO coverages deposited on Ag(100) at 300 K: (a) 0.3 ML, (b) 0.8 ML, (c) 1.0 ML, (d) 1.1 ML, (e) 1.4 ML, and (f) 2.0 ML. The characteristic NiO monolayer vibration is gray, whereas second layer vibrations are yellow.

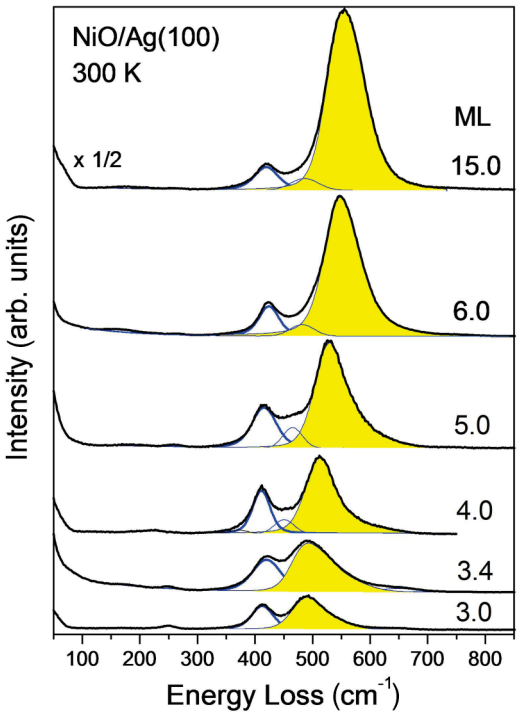


FIG. 5. The HREEL spectra of Ni(100) films with different thicknesses (indicated in the figure), as grown on Ag(100) at 300 K. The FK phonon polariton is marked in yellow.

spectra for higher NiO thickness. On the other hand, for the saturated $c(2 \times 2)$-O coverage on Ni(001), the vertical oxygen vibration has been found at 318 $cm^{-1}$ [28], close to our measurement for the "precursor" NiO phase below 1 ML (Fig. 4). By analogy, the peak at 300 $cm^{-1}$ for this NiO monolayer phase can be attributed to the vertical optical Ni-O phonon with a dominating oxygen amplitude, whereas the peak at about 125 $cm^{-1}$ corresponds to a parallel (in-plane) vibration.

Figure 4(d) shows the HREEL spectrum for the initial stage of growth of the second layer of NiO. It is accompanied by an increase of the peak at 417 $cm^{-1}$ and a 5 $cm^{-1}$ downshift of the corresponding Ni-O vibration at ~300 $cm^{-1}$ of the first monolayer. Interestingly, a small amount of second layer NiO (about 0.1 ML) causes a large screening of the vibrational structure of the first monolayer [Fig. 4(d)]. Indeed, the energy losses of different coverages within the second monolayer [Figs. 4(e) and 4(f)] have intensities up to 10 times greater than that of 1 ML [Fig. 4(c)], which is also evident from Fig. 3. The energy loss spectrum of the second layer is characterized by a phonon polariton, with a slightly coverage dependent frequency of 444 to 449 $cm^{-1}$ with increasing NiO thicknesses between 1.4 and 2 ML [Figs. 4(e) and 4(f)]. Additionally, the NiO(001) bilayer spectra show a low-energy shoulder of the dominant peak. The spectra can be reliably fitted by introducing a peak at about 400 $cm^{-1}$ that is attributed to a Ni-O vibration in analogy with the microscopic Wallis mode characteristic for thick NiO layers [6]. Above 1.4 ML, the frequency of this peak increases from 400 up to 405 $cm^{-1}$ when the growth of the second NiO layer is completed. As mentioned above, the monolayer features are strongly suppressed for coverages above 1.4 ML.

### C. NiO(001) films beyond 2 ML

In Fig. 5, the HREEL spectra for NiO films in the range of 3–15 ML are presented. Starting from 3 ML, the dominant FK phonon polariton and the Wallis mode are well separated at ~490 and 413 $cm^{-1}$, respectively (Fig. 5, bottom spectrum). With increasing NiO coverage, the FK frequency increases, while that of the Wallis mode is not sensitive to the layer thickness. The contribution of the FK phonon polariton to the spectra is in yellow in Fig. 5. For the low NiO thicknesses, its peak is broad and asymmetric, while at higher NiO coverages of 15 ML, it becomes more symmetrical but still with a large FWHM as compared to that of the Wallis phonon loss. This result is in agreement with our observation for 25 ML thick NiO(001) films [6]. As discussed there, the broad line shape of the FK phonon-polariton loss results from a splitting of the bulk optical phonon due to the magnetic order in the antiferromagnetic state of NiO. In Table I, the frequencies of both FK and Wallis modes are summarized for different NiO film thicknesses.

In the low-frequency region, a number of weak phonon features appears with frequencies also depending on the NiO film thicknesses. A narrow peak at ~250 $cm^{-1}$ grows with increasing coverage within the third monolayer (lowest two spectra in Fig. 5) that is absent for 2 ML films (Fig. 4). It is also present for thicker NiO films and characterizes a

TABLE I. The NiO(001) on Ag(001): the thickness-dependent frequencies of the Wallis phonon and the FK phonon-polariton. NiO(001) bulk TO and LO phonon frequencies at appropriately selected standing wave wave vectors (see text) are taken from literature [29]. Error bars for all surface phonon data are 1 $cm^{-1}$; standing wave data are $\pm 2$ $cm^{-1}$.

| NiO thickness | Wallis | FK | Standing wave [29] | |
|---|---|---|---|---|
| (ML) | mode ($cm^{-1}$) | mode ($cm^{-1}$) | TO ($cm^{-1}$) | LO ($cm^{-1}$) |
| 2 | 405 | $447 \pm 3.0$ | 414 | 562 |
| 3 | 413 | 490 | 395 | 571 |
| 4 | 413 | 514 | 391 | 573 |
| 5 | 416 | 529 | 388 | 574 |
| 6 | 422 | 542 | 387 | 575 |
| 8 | 424 | 546 | 387 | 577 |
| 15 | 421 | 554 | 387 | 577 |
| 25 | 425 | 559 | 387 | 577 |

phonon feature with resonance character at the Γ point of the surface Brillouin zone (SBZ) [6]. For thicknesses above 5 ML, faint low-intensity losses in the region of 170 to 200 $cm^{-1}$ characterize surface resonance phonons by analogy with bulklike NiO(001) [6].

### D. Temperature-dependent morphology changes

As we show in the following, the thermal stability of the NiO film increases strongly with the film thickness. The lowest thermal stability is observed for the submonolayer range.

Figure 1 shows that at the beginning of NiO deposition the (00) spot intensity decreases strongly indicating a highly inhomogeneous surface layer as compared to the bare substrate surface. Similarly, the reflectivity of elastically scattered 4 eV electrons in HREELS is drastically reduced upon deposition of 0.1–0.15 ML of NiO as compared to the clean surface. Under these conditions, no losses are resolved in the spectrum as shown in Fig. 6(a). Annealing to 670 K causes a significant increase (∼50 times) of the peak intensity of elastically scattered electrons and energy losses are clearly observable [Fig. 6(b)]. The spectrum exhibits an energy loss at about 145 $cm^{-1}$ characteristic for the clean Ag(001) surface [22], as well as two strong peaks at 424 and 540 $cm^{-1}$ characteristic for the Wallis mode and the FK phonon polariton of small NiO islands. The HREEL spectrum in Fig. 6(b) contains also a weak peak at about 260 $cm^{-1}$ that has been also observed for NiO films of 3 and 4 ML (see Fig. 4). According to previous STM studies, annealing to 400 K leads to the transformation of the monolayer phase into 2 and 3 ML high NiO islands that are partially embedded into the Ag surface [13]. Also, Caffio *et al.* have concluded that an annealing process to 620 K causes a formation of bilayer NiO islands [20]. However, the shape of the vibrational structure induced by annealing at 670 K [Fig. 6(b)] is similar to a 4 ML NiO film (Fig. 5), whereas its frequency matches better with 6 ML according to Table I. The FK-related peak is almost symmetric, suggesting a high thickness of the formed NiO islands (see Sec. III A).

Upon annealing the full first monolayer of NiO on Ag(001), noticeable changes occur only for temperatures above 500 K (Fig. 7). The complex vibrational spectrum upon annealing to

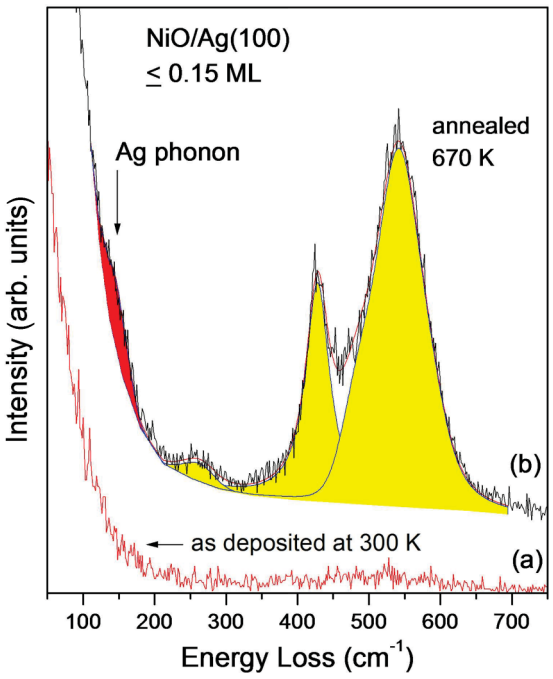


FIG. 6. Vibrational spectra of ⩽0.15 ML NiO coverage deposited on Ag(100) at 300 K (a) and after annealing at 670 K (b). NiO thin film and substrate phonons are marked in yellow and red.

550 K can be successfully fitted with several contributions (Fig. 7). There are islands with local coverage of 1 ML characterized by an intense loss at ∼300 $cm^{-1}$, whereas the broad FK peak at 463 $cm^{-1}$ indicates the presence of islands with local thickness of mainly 2 ML according to Table I. Its shift to higher frequency suggests the existence of some NiO islands of 3 ML. This can also explain the relative intense and broad Wallis loss at about 393 $cm^{-1}$, as compared to the 2 ML NiO film in Fig. 4(f), suggesting a Wallis phonon contribution from the 3 ML islands. This is in agreement with previous studies [10,12,20] showing that annealing of the NiO monolayer leads to formation of NiO bilayer islands. Also, STM has identified 3 ML NiO islands under similar conditions [13]. The low-intensity peak at about 235 $cm^{-1}$ falls in a frequency region where characteristic NiO phonon exists [see Fig. 6(b)]. Upon annealing to 600 K, the NiO monolayer film is completely transformed into 2 and 3 ML (1 × 1) islands with characteristic Wallis phonon contributions at 393 and 413 $cm^{-1}$, respectively, and a broad asymmetrical FK loss at ∼460 $cm^{-1}$ (top spectrum in Fig. 7). This is in agreement with a recent STM study [14], where relatively large (1 × 1) NiO islands embedded into the Ag surface have been observed after annealing at 600 K.

Interestingly, a continuous 2 ML NiO film is stable up to 600 K, as is inferred from the results of Fig. 8. Its Wallis and FK losses at ∼400 and 450 $cm^{-1}$, respectively, dominate in the spectra (see light gray in Fig. 8). After annealing at 650 K, a Wallis phonon of 3 ML NiO islands appears clearly as a new contribution (see yellow in Fig. 8). The FK loss peak is slightly shifted to 460 $cm^{-1}$, and it gets broader and asymmetric for this mixed 2 and 3 ML NiO island morphology (marked in yellow-gray color). The FK frequency continues to increase

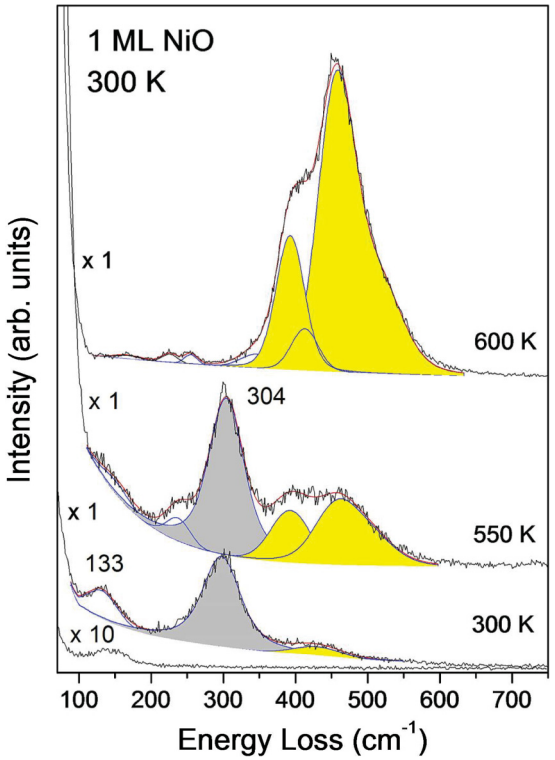


FIG. 7. The HREEL spectra of clean Ag(100) (bottom), of 1 ML NiO on Ag(001) as grown at 300 K, and upon subsequent annealing to 550 and 600 K (from bottom to top). The characteristic NiO monolayer vibration is colored gray, whereas second and higher layer vibrations are yellow.

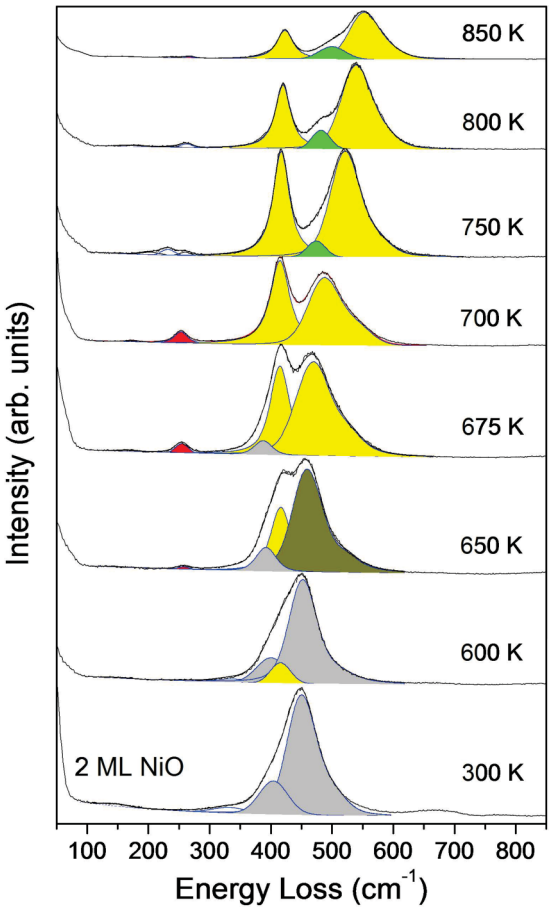


FIG. 8. Thermal evolution of HREEL spectra for a 2 ML NiO(100)-(1 × 1) film grown at 300 K. The subsequent annealing temperatures are indicated on the right. The NiO bilayer vibrations are gray, whereas FK and Wallis mode vibrations for three or more NiO layers are yellow. For additional features in red and green, see text.

with the annealing temperature to ∼470 $cm^{-1}$, reaching a value of ∼490 $cm^{-1}$ characteristic for the bare 3 ML NiO film at 700 K (see Table I). Note also that the low-energy phonon feature at about 255 $cm^{-1}$ (see red in Fig. 8) characteristic for the 3 ML NiO film is clearly visible (see also Fig. 9). Therefore, we conclude that relatively large 3 ML NiO islands are formed by annealing at 700 K. Increasing the annealing temperature above 700 K leads to a sequentially increase in the FK frequency up to 553 $cm^{-1}$ at 850 K (top spectrum in Fig. 8). This correlates with a sequential transformation to islands with higher thickness but with reduced lateral dimensions. The data of Table I suggest that the FK frequency measured at 850 K corresponds to NiO islands with a local thickness of ∼15 ML. The additional feature at 470–490 $cm^{-1}$ (see green) appears at temperatures above 750 K and is clearly visible at 800 K in Fig. 8. Such a contribution has been also necessary to introduce in a fitting of HREEL spectra of thick NiO films above 4 ML (Fig. 5), probably, indicating the presence of islands with local thicknesses of 2–3ML (see also Sec. IV A).

Figure 9 demonstrates that a continuous 3 ML film is stable up to 700 K. Up to 750 K, the shape of the HREELS spectrum does not change significantly. However, the intensity of the elastically scattered electrons, as well as the phonon features increases strongly with annealing temperature by a factor of about six. This increase in intensity corresponds to an increased reflectivity due to an improved long-range order of the NiO(001) film. Figure 9(b) shows this increase for the elastic peak intensity $I_0\,(T)$ normalized to the intensity at 300 K, $I_0$ (300 K). In contrast, the energy loss data in Fig. 9(a) are normalized to the elastic peak intensity at a given annealing temperature and, therefore, do not show the reflectivity increase.

Above 700 K, the growth of thicker NiO islands begins, and at 800 K, a mixture of 3 and 4 ML islands exists, as evidenced by the appearance of a high frequency peak at about 520 $cm^{-1}$ (see Table I). Subsequent heating to 850 K leads to the almost disappearance of the 3 ML NiO regions. The FK phonon-polariton frequency is shifted further to 531 $cm^{-1}$. According to the data in Table I, this higher frequency corresponds to NiO islands of 5 ML. The formation of thicker NiO islands of 4–5 ML above 750 K is accompanied by an intensity decrease of elastically scattered electrons due to the formation of layer vacancies in the NiO film.

For NiO layers with an initial thickness larger than 4 ML, annealing up to 850 K does not lead to new vibrational features in HREELS (not shown here). However, Wallis and FK phonon peaks are better resolved because the intensity of the ∼480 $cm^{-1}$ peaks between them decreases upon annealing. Also, the electron reflectivity increases, which is ascribed to an improved long-range order of the NiO(001) films.

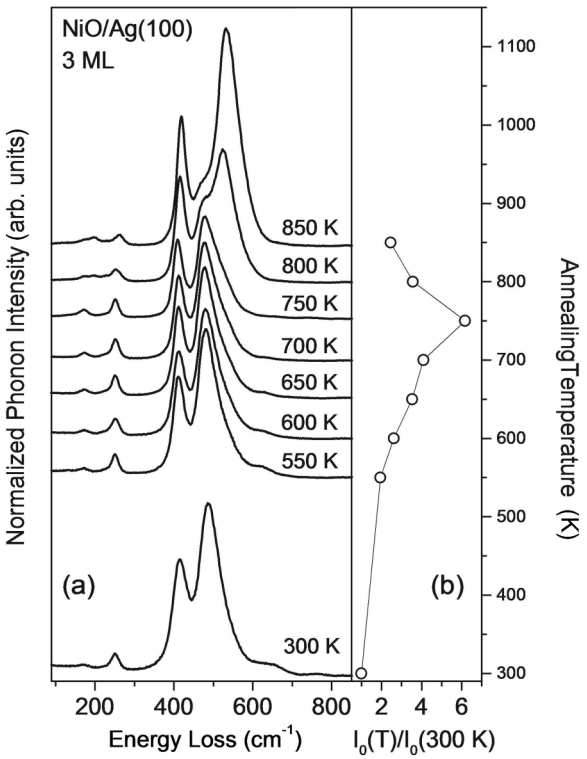


FIG. 9. (a) Thermal evolution of HREEL spectra for a 3 ML NiO(100)-(1 × 1) film grown on Ag(100) at 300 K. The subsequent annealing temperatures are indicated in the figure. (b) Intensities $I_0$ (T) of elastically scattered electrons at different annealing temperatures normalized to the intensity $I_0$ (300 K) at NiO deposition temperature.

## IV. DISCUSSION

### A. Surface vibrations of NiO films

The first monolayer of NiO on Ag(001) forms a uniaxially compressed (2 × $n$) structure, which is often termed (2 × 1) "precursor" NiO phase, as has been discussed in Sec. III A. The vibrational properties are characterized by a vertical Ni-O and an in-plane vibration at 300 and 125 $cm^{-1}$, respectively. These significantly lower frequencies as compared to thicker NiO films are in the range of frustrated translations (perpendicular and parallel motions) of adsorbed gas particles, e.g., the vertical Ni-O phonon frequency is close to the stretching vibration at 318 $cm^{-1}$ of atomic oxygen on Ni(001) [28]. The significantly different vibrational fingerprint of the first NiO layer supports the oxide atypical character of this precursor state.

The NiO(001)-(1 × 1) bilayer is characterized by higher frequency vibrations of 450 and 405 $cm^{-1}$. These frequencies are still lower than those of corresponding FK and Wallis modes (558 and 430 $cm^{-1}$) for thick NiO films. However, these modes are already characteristic for a NiO(001) oxide, which indicates that growth of the second layer restructures also the first layer underneath. Additionally, the bilayer exhibits a broad vibration at ∼150 $cm^{-1}$ that is absent for bulklike NiO(001) [6].

The Wallis and the FK phonon-polariton frequencies are well separated for NiO(001)-(1 × 1) films, with a minimal thickness of 3 ML, which indicates the beginning of the development of a bulklike phonon structure. For 3 ML thick films, additional peaks at ∼170 and 248 $cm^{-1}$ are observed, which are characteristic for this thickness. Although they fall in an energy range where surface resonances have been observed for NiO(001) [6], their strong and well-defined appearance only at 3 ML points to an NiO interface mode that is screened for thicker films and not yet developed for the NiO bilayer.

The characteristic phonon structures for NiO(001) films with thicknesses above 4 ML are similar, but a thickness-dependent increase in intensity and frequency of the FK phonon is observed. The frequency difference between FK and Wallis losses varies between 80 and 130 $cm^{-1}$, depending on the film thickness (Table I). A detailed analysis of this energy loss region, as discussed for Fig. 5, finds another feature at 450–490 $cm^{-1}$. Most prominently, it is seen for 4 and 5 ML films (Fig. 5). According to Table I, these frequencies correspond to FK modes of 2–3 ML thick NiO films. In STM studies of NiO(001) nanosize islands, Steurer *et al.* propose a structural model of island boundaries, including partially embedded line of NiO bilayer [14]. By analogy, the vibrational peak at 450–490 $cm^{-1}$ is tentatively assigned to 2–3 ML thick NiO structures, e.g., at the rim of thicker islands.

### B. Thickness-dependent vibrational frequencies and intensities

The frequency and intensity of the FK mode depend strongly on the NiO film thickness, as is summarized in Fig. 10. The figure shows a strong FK phonon shift of about 80 $cm^{-1}$ in the thickness range of 2–5 ML. Characteristic changes of the LEED pattern are observed between 5 and 15 ML (Fig. 2), and they are ascribed to structural relaxation processes, which are linked to the formation of the NiO mosaic structure [15]. The FK frequency increases only moderately by 20 $cm^{-1}$ between 5 and 15 ML NiO thickness. Above 15 ML, the FK frequency remains constant and is comparable to the value for bulklike NiO(001) of 558.5 $cm^{-1}$ (measured for 50 ML thick NiO), as shown in Fig. 10. The intensity of the FK mode increases strongly with film thickness. The dielectric theory, which describes the electron energy loss function for specular scattering conditions, predicts an initially linear increase in the FK intensity [black solid line in Fig. 10(b)] before it levels off for thick films. The linear intensity increase stems from the increasing number of oscillators within the film, whereas its saturation is due to finite probing depth of the surface phonon polariton. The experimentally observed initial increase of the FK intensity with thickness relative to the intensity of the specular zero-loss peak deviates slightly from the linear behavior. It signals a different influence of surface defects (especially for not fully closed layers) on the intensity of the specular beam and of the FK phonon loss feature.

The frequency of the Wallis mode is less sensitive to film thickness and stress. It changes continuously from 405 $cm^{-1}$ at 2 ML to 430 $cm^{-1}$ for thick NiO films (Fig. 10). Whereas the Wallis mode intensity stays constant above 5 ML, we find an approximately linear increase between 2 and 5 ML. This behavior is depicted by the dashed red line in Fig. 10.

As we have shown earlier, the dielectric properties and especially the surface loss function of thick NiO films are

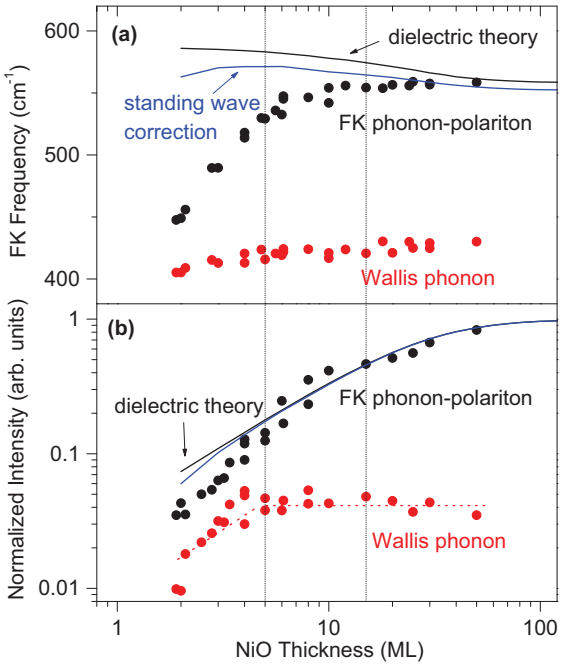


FIG. 10. Frequency (a) and intensity (b) of the FK phonon polariton (black solid circles) and the Wallis phonon (red solid circles) for NiO(001)-(1 × 1) films on Ag(001). The calculated frequency shift of the FK mode due to the dielectric theory without (black) and with standing wave corrections (blue) is shown by solid lines. Three different thickness regimes (below 5, 5–15, and above 15 ML) are indicated by vertical lines. The intensity in (b) is normalized to the zero-loss specular beam intensity for each layer thickness.

well described by the respective bulk properties [6]; NiO is characterized by a high-frequency permittivity $\varepsilon_\infty = 5.25$ and two independent transversal optical eigenfrequencies of 399 and 563 cm$^{-1}$. It can be well described by a generalized oscillator model with damping terms of 14 and 68 cm$^{-1}$, respectively [6]. These values lead to a surface loss function, which gives a frequency of the FK mode of 559 cm$^{-1}$ for the limit of thick films, in good agreement with the experimental value. For ultrathin films, however, there are three additional effects to consider:

(i) The surface loss function and, especially, the FK mode are described by the effective dielectric response of the combination of thin film plus substrate. This can be analytically expressed for a planar thin film geometry by

$$\varepsilon_{\mathrm{surf}}(\omega) = \varepsilon \coth(qd) - \frac{\varepsilon/\sinh(qd)}{\varepsilon \coth(qd) + \varepsilon_{\mathrm{sub}}}, \quad (1)$$

where the quantity $d$ is the thickness of the NiO film in integer multiples of 2.09 Å, half the bulk lattice parameter of NiO. The phonon wave vector is denoted by $q$ and the frequency-dependent NiO bulk dielectric function by $\varepsilon$. The metallic response of the Ag(001) substrate is given by $\varepsilon_{\mathrm{sub}} = \frac{-\omega_p{}^2}{\omega^2 + i\,\gamma\,\omega}$ with a plasma frequency of 3.9 eV and a damping of 0.02 eV according to Ref. [30]. In the planar film geometry, we apply the dielectric theory similarly, as developed by Lambin *et al.* [31,32], which allows a quantitative calculation of the experimentally observed energy-loss spectrum from the surface loss function and vice versa. The zero-temperature electron energy loss probability is given by [31,32],

$$P_{cl}(\omega) = \frac{e^2}{4\pi\varepsilon_0\hbar v_\perp}\frac{2}{\pi^2}\iint_{q_\parallel}\frac{q_\parallel {v_\perp}^3}{[(q v_\parallel - \omega)^2 + (q_\parallel v_\perp)^2]^2} \times \mathrm{Im}\left[\frac{-1}{\varepsilon_{\mathrm{surf}}(\omega)+1}\right] dq_\parallel, \quad (2)$$

where $v_\parallel$ and $v_\perp$ are the components of the electron velocity parallel and perpendicular to the surface given by the primary energy and the impact angle of the electrons. The integration range covers all wave vectors according to the acceptance aperture of the energy analyzer. In our case, the acceptance aperture is circular, with an acceptance angle of ±2° that leads to an integration up to $q_\parallel = 0.036\,\text{Å}^{-1}$ for 4 eV primary energy. The integrand consists of the product of surface loss function $\mathrm{Im}[\frac{-1}{\varepsilon_{\mathrm{surf}}(\omega)+1}]$ and the (experimentally defined) kinematic factor, as reported earlier [31,32].

(ii) The second correction concerns the TO and LO frequencies. Whereas the bulk phonon frequencies for $k_\perp = 0$ and $k_\parallel = 0$ enter into the dielectric response for an infinite thick film, the bulk phonon frequencies at $k_\perp = 2\pi/d$ and $k_\parallel = 0$ have to be considered for a finite film thickness $d$ due to the standing wave nature of these phonons in the direction along the film normal [33,34]. Depending on the bulk TO and LO dispersions, this might lead to a significant correction for ultrathin films. The NiO thickness-dependent TO and LO phonon frequencies are taken according to the NiO bulk phonon dispersion in Ref. [29] and are summarized in the last two columns of Table I. Based on the inelastic neutron scattering data, the LO phonon shifts from 570 cm$^{-1}$ at the Γ point to 475 cm$^{-1}$ at the $X$ point [29]. At half way Γ$X$, the LO phonon is shifted to 520 cm$^{-1}$. For standing waves of films with thickness d of 2 ML and above, the dispersion along the first 25% of Γ$X$ is relevant only. This allows estimating the maximum downshift to 3% for 2 ML. Therefore, this correction leads only to a minor change of the FK frequency for thicknesses below 4 ML, as indicated in Fig. 10(a) by a blue line. Note that for NiO, the standing wave corrections are significantly smaller than for LiBr and MgO [33,34] due to smaller dispersion of the TO and LO phonons of NiO. A small constant offset (6 cm$^{-1}$) of the standing wave correction [blue line in Fig. 10(a)] as compared to the dielectric theory (black line) arises purely from the different TO bulk frequencies in Refs. [29,35], respectively.

(iii) The largest contribution to the observed phonon softening for ultrathin films arises from the strained growth of NiO. Due to the lattice mismatch of −2%, the pseudomorphic NiO growth in the region between 2 and 5 ML leads to a significant stress of order −5.8 GPa, as has been determined quantitatively by

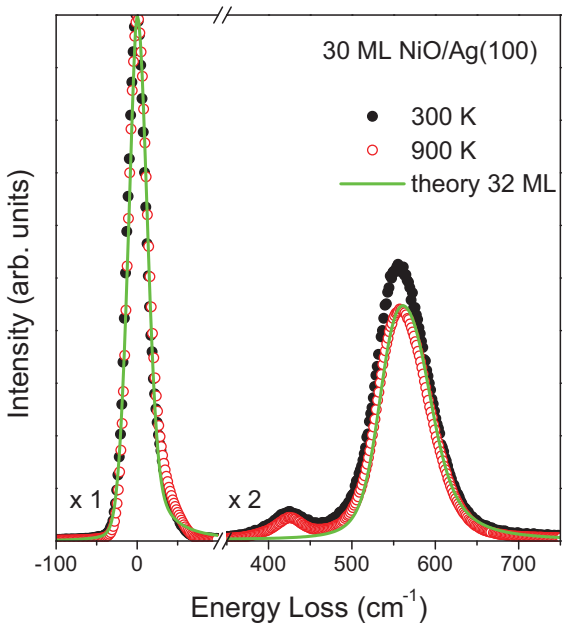


FIG. 11. Experimental HREEL spectrum for a 32 ML NiO(100)-(1 × 1) thin film (black solid circles) and upon annealing at 900 K (open red circles). The solid green line shows the calculated energy loss function based on dielectric theory for one oscillator with bulk TO and LO frequencies downshifted by 6 $cm^{-1}$ and bulk phonon linewidths.

the crystal bending technique [4]. For the subsequent growth between 5 and 15 ML, the further stress is reduced. This is ascribed to the structural relaxations into a mosaic structure (5 ML), and a long-range Moiré structure (15–30 ML), as observed by LEED (Fig. 2). Based on this observation, we suggest that film stress is the dominant factor, which leads to the observed softening of the FK mode. Note that the phonon shift due to the finite thickness of the NiO layer (due to standing waves within the film and due to the dielectric response from the metallic substrate) is rather small, as shown by the solid lines in Fig. 10.

For NiO films well above 15 ML, the dielectric theory predicts excellently the energy loss function based on NiO bulk phonon data. Figure 11 illustrates this for a 32 ML NiO(001) film, which has been annealed to 900 K. The green solid line describes the calculate HREELS loss function, which has been convoluted with the instrumental broadening. The latter is extracted from the shape of the elastic peak. The energy, width, and intensity of the FK phonon are well described by the bulk phonon properties of Ref. [35]. Analogously, the HREEL spectrum can be converted back to the complex dielectric function $\varepsilon(\omega)$ for the near surface region (not shown here). This allows extracting the surface optical response in the region of 30 to 1000 $cm^{-1}$ (1 to 30 THz) with high sensitivity and accuracy.

## V. CONCLUSIONS

The growth of NiO films on Ag(001) at 300 K has been studied by HREELS to obtain information about phonon properties, geometrical structure, and growth mode of the oxide layer. These characteristics depend strongly on NiO thickness, and four NiO coverage regimes are identified. In the first NiO thickness region of 0–2 ML, an uniaxially compressed "(2 × 1)" NiO monolayer phase exists that is characterized by a perpendicular Ni-O vibration at ∼300 $cm^{-1}$ and a low-frequency vibration at 125 $cm^{-1}$. This "precursor" phase covers almost completely the Ag(001) surface at 1 ML coverage. Simultaneously, NiO(001) bilayer islands nucleate covering uniformly the surface at 2 ML oxide thickness. For this bilayer film, the dominant phonon mode, the FK phonon polariton, has a significantly higher frequency of ∼450 $cm^{-1}$. Within the second region of 2–5 ML, compressed NiO(001) films grow pseudomorphically preserving the Ag(001) surface lattice parameters. A phonon structure similar to that of bulklike NiO(001) begins to form with increasing thickness from 3 NiO ML on. The frequencies of its FK phonon and a second dipole-active, but microscopic Wallis mode, are detected at ∼490 and ∼413 $cm^{-1}$, respectively.

Characteristic mosaic diffraction patterns are observed for NiO(001) film with thicknesses within the third region of 5–15 ML. These diffraction features provide evidence for structural relaxation processes in the growing oxide. Here, the frequency of the FK phonon-polariton changes from 530 to 555 $cm^{-1}$, with increasing NiO thickness. The Wallis mode frequency remains almost constant. The fourth coverage region is characterized by fully relaxed NiO(001) at thicknesses above 15 ML. Beginning from 15 ML NiO, the FK frequency increases with increasing oxide thickness to ∼560 $cm^{-1}$ for thick NiO films of 40–50 ML, resembling NiO bulk properties.

The thermal stability of the as-grown NiO film depends strongly on the film thickness. Already at 500 K, submonolayer and monolayer of NiO on Ag(001) start to restructure. At 600 K, they form NiO(001)-(1 × 1) islands with thicknesses, of at least 3–5 ML, depending on the initial film thickness. The temperatures at which significant lateral oxide transport sets in are shifted to higher values of 600, 700, and ∼900 K with increasing NiO thicknesses of 2, 3, and 4 ML, respectively. Annealing at temperatures below these threshold values does not change the FK frequency. However, it results in a surface ordering that leads to a strong increase of the electron reflectivity, as measured by HREELS.

The quantitative comparison of the experimental data with the calculated HREELS loss function, based on the dielectric theory, reveals bulklike phonon properties for NiO(001) thin films of thicknesses above 15 ML. However, for NiO(001)-(1 × 1) films of 2 to 5 ML, a strong phonon softening is found that is attributed to the surface stress that results from the lattice mismatch. With forthcoming theoretical descriptions, we speculate that NiO on Ag(001) might be the first prime candidate for a quantitative understanding of the interrelation between surface stress and phonon softening in binary oxides.

## ACKNOWLEDGMENTS

Financial support has been provided by the Deutsche Forschungsgemeinschaft through Sonderforschungsbereich SFB-762 "Functionality of Oxidic Interfaces".

[1] J. H. Haeni, P. Irvin, W. Chang, R. Uecker, P. Reiche, Y. L. Li, S. Choudhury, W. Tian, M. E. Hawley, B. Craigo, A. K. Tagantsev, X. Q. Pan, S. K. Streiffer, L. Q. Chen, S. W. Kirchoefer, J. Levy, and D. G. Schlom, Nature (London) **430**, 758 (2004).
[2] W. Eerenstein, N. D. Mathur, and J. F. Scott, Nature (London) **442**, 759 (2006).
[3] D. A. Tenne, A. Bruchhausen, N. D. Lanzillotti-Kimura, A. Fainstein, R. S. Katiyar, A. Cantarero, A. Soukiassian, V. Vaithyanathan, J. H. Haeni, W. Tian, D. G. Schlom, K. J. Choi, D. M. Kim, C. B. Eom, H. P. Sun, X. Q. Pan, Y. L. Li, L. Q. Chen, Q. X. Jia, S. M. Nakhmanson *et al.*, Science **313**, 1614 (2006).
[4] A. Dhaka, D. Sander, H. L. Meyerheim, K. Mohseni, E. Soyka, J. Kirschner, W. A. Adeagbo, G. Fischer, A. Ernst, and W. Hergert, Phys. Rev. B **84**, 195441 (2011).
[5] J. Premper, D. Sander, and J. Kirschner, Appl. Surf. Sci. **335**, 44 (2015).
[6] K. L. Kostov, S. Polzin, S. K. Saha, O. Brovko, V. Stepanyuk, and W. Widdra, Phys. Rev. B **87**, 235416 (2013).
[7] K. L. Kostov, S. Polzin, F. O. Schumann, and W. Widdra, Surf. Sci. **643**, 23 (2016).
[8] K. Marre and H. Neddermeyer, Surf. Sci. **287-288**, 995 (1993).
[9] K. Marre, H. Neddermeyer, A. Chassé, and P. Rennert, Surf. Sci. **357-358**, 233 (1996).
[10] Th. Bertrams and H. Neddermeyer, J. Vac. Sci. Technol. B **14**, 1141 (1996).
[11] I. Sebastian, Th. Bertrams, K. Meinel, and H. Neddermeyer, Faraday Discuss. **114**, 129 (1999).
[12] M. Caffio, A. Atrei, B. Cortigiani, and G. Rovida, J. Phys.: Condens. Matter **18**, 2379 (2006).
[13] S. Großer, C. Hagendorf, H. Neddermeyer, and W. Widdra, Surf. Interface Anal. **40**, 1741 (2008).
[14] W. Steurer, F. Allegretti, S. Surnev, G. Barcaro, L. Sementa, F. Negreiros, A. Fortunelli, and F. P. Netzer, Phys. Rev. B **84**, 115446 (2011).
[15] J. Wollschläger, D. Erdös, H. Goldbach, R. Höpken, and K. M. Schröder, Thin Solid Films **400**, 1 (2001).
[16] M. Caffio, B. Cortigiani, G. Rovida, A. Atrei, C. Giovanardi, A. di Bona, and S. Valeri, Surf. Sci. **531**, 368 (2003).
[17] K. L. Kostov, M. Gzell, P. Jakob, T. Moritz, W. Widdra, and D. Menzel, Surf. Sci. **394**, L138 (1997).
[18] K. L. Kostov, D. Menzel, and W. Widdra, Phys. Rev. B **61**, 16911 (2000).
[19] K. L. Kostov, W. Widdra, and D. Menzel, J. Phys. Chem. B **108**, 14324 (2004).
[20] M. Caffio, B. Cortigiani, G. Rovida, A. Atrei, and C. Giovanardi, J. Phys. Chem. **108**, 9919 (2004).
[21] J. Wollschläger, D. Erdös, and K.-M. Schröder, Surf. Sci. **402-404**, 272 (1998).
[22] I. Amidror, *The Theory of the Moiré Phenomenon*—Volume I: Periodic Layers (Springer, London, UK, 2009).
[23] R. F. Wallis, D. L. Mills, and A. A. Maradudin, in *Localized Excitation in Solids*, edited by R. F. Wallis (Plenum, New York, 1968), p. 403.
[24] R. Fuchs and K. L. Kliewer, Phys. Rev. **140**, A2076 (1965).
[25] K. L. Kliewer and R. Fuchs, Phys. Rev. **144**, 495 (1966).
[26] M. Rocca, L. Savio, L. Vattuone, U. Burghaus, V. Palomba, N. Novelli, F. Buatier de Mongeot, U. Valbusa, R. Gunnella, G. Comelli, A. Baraldi, S. Lizzit, and G. Paolucci, Phys. Rev. B **61**, 213 (2000).
[27] K.L. Kostov, S. Polzin, and W. Widdra, J. Phys.: Condens. Matter **23**, 484006 (2011).
[28] T. S. Rahman, D. L. Mills, J. E. Black, J. M. Szeftel, S. Lehwald, and H. Ibach, Phys. Rev. B **30**, 589 (1984).
[29] W. Reichardt, V. Wagner, and W. Kress, J. Phys. C. **8**, 3955 (1975).
[30] G. B. Irani, T. Huen, and F. Wooten, Phys. Rev. B **3**, 2385 (1971); H. Ehrenreich and H. R. Philipp, Phys. Rev. **128**, 1622 (1962); E. Furtak and D. W. Lynch, Phys. Rev. Lett. **35**, 960 (1975).
[31] Ph. Lambin, J. P. Vigneron, and A. A. Lucas, Comp. Phys. Commun. **60**, 351 (1990).
[32] Ph. Lambin, J. P. Vigneron, and A. A. Lucas, Phys. Rev. B **32**, 8203 (1985).
[33] P. Senet, Ph. Lambin, and A. A. Lucas, Phys. Rev. Lett. **74**, 570 (1995).
[34] L. Savio, E. Celasco, L. Vattuone, M. Rocca, and P. Senet, Phys. Rev. B **67**, 075420 (2003).
[35] C. Kant, F. Mayr, T. Rudolf, M. Schmidt, F. Schrettle, J. Deisenhofer, and A. Loidl, Eur. Phys. J. Spec. Top. **180**, 43 (2009).